N O T I C E

THIS DOCUMENT HAS BEEN REPRODUCED FROM
MICROFICHE. ALTHOUGH IT IS RECOGNIZED THAT
CERTAIN PORTIONS ARE ILLEGIBLE, IT IS BEING RELEASED
IN THE INTEREST OF MAKING AVAILABLE AS MUCH
INFORMATION AS POSSIBLE

MODELING OF THIN-FILM GaAs GROWTH

By

John H. Heinbockel, Principal Investigator

Progress Report
For the period May 15 to September 15, 1981

October 1981

DEPARTMENT OF MATHEMATICAL SCIENCES
SCHOOL OF SCIENCES AND HEALTH PROFESSIONS
OLD DOMINION UNIVERSITY
NORFOLK, VIRGINIA

MODELING OF THIN-FILM GaAs GROWTH

By

John H. Heinbockel, Principal Investigator

Progress Report
For the period May 15 to September 15, 1981

October 1981

TABLE OF CONTENTS

LIST OF TABLES

LIST OF FIGURES

MODELING OF THIN-FILM GaAs GROWTH

By

John H. Heinbockel[*]

SUMMARY

A solid-on-solid Monte Carlo model is constructed for the simulation of crystal growth. The model assumes thermally accommodated adatoms impinge upon the surface during a Δt time interval. The surface adatoms are assigned a random energy from a Boltzmann distribution, and this energy determines whether the adatoms evaporate, migrate, or remain stationary during the Δt time interval. For each addition or migration of an adatom, potential wells are adjusted to reflect the absorption, migration, or desorption potential changes.

INTRODUCTION AND STATEMENT OF PROBLEM

Numerous methods have been applied to obtaining thin film, single crystals of GaAs, including free-standing wafers, peal films removed from a single crystal substrate, and films grown on light-weight substrates. One of the most promising methods is a version of the last technique called "graphoepitaxy." It is generally known that overlayers of crystalline materials deposited upon smooth microcrystalline substrates tend to be more or less randomly polycrystalline. The absence of long-range order in the microcrystalline substrate is reflected in the absence of long-range order in the overlayer. The basic concept of graphoepitaxy is that, by intro-ducing an artificial surface relief structure having a long-range order on a microcrystalline substrate, long-range order can be induced in an overlayer. In other words, a crystalline film can be grown on a microcrystalline substrate.

---

[*]Professor, Department of Mathematical Sciences, Old Dominion University, Norfolk, VA 23508.

In order to be able to study the dynamics of crystal growth on gratings, a more detailed model of crystal growth is needed. The following is the development of a solid-on-solid (SOS) model for the simulation of molecular exchange between the solid and vapor phases whereby dynamics are introduced into the model by a random deposition, migration, and desorption of adatoms at random surface positions.

LIST OF SYMBOLS

a_o	lattice constant (nm)
M	size of square array
I	integer position
$H(I)$	height at position I
ϕ_o	potential energy change at site I caused by adatom deposition (eV)
ω_i	($i = 1, \ldots, 8$) potential energy changes at sites neighboring I (eV)
Δt	time interval (sec)
$E = E(I)$	random energy assigned to site I (eV)
$U(I)$	total energy associated with site 1 (eV)
U_o	potential energy at site I (eV)
U_e	evaporation level (eV)
U_m	migration level (eV)
ϕ_1	nearest neighbor potential change
ϕ_2	second nearest neighbor potential change
ϕ_3	third nearest neighbor potential change
$\phi^*, R^*,$ n_o, m_o	Mie potential parameters
U_{ms}	migration level (substrate) (eV)
U_{es}	evaporation level (substrate) (eV)

2

U_{os} potential at site I (substrate) (eV)

K   Boltzmann constant (8.6×10^{-5}) (eV/°K)

T   absolute temperature (°K)

α_2, α_3 scale factors for Mie potentials

$U_{nCLUSTER}(ijk)$ potential energy on (ijk) face for cluster of n-adatoms (eV)

E_{median} median energy for Boltzmann distribution

n_1, m_1, ℓ_1 integers associated with (ijk) orientation

$\Delta U_m = U_m - U_o$ surface diffusion activation energy (eV)

$\Delta U_e = 0 - U_o$ evaporation energy (eV)

T_r reference temperature (°K)

R   uniform random number

ν_1, ν_o frequency factors

D_s diffusion coefficient

X_s mean adatom displacement

R_d deposition rate

R_e evaporation rate

R_g vertical growth rate

P   supersaturated vapor pressure

P_e equilibrium pressure

MODELING OF GaAs CRYSTAL GROWTH

Structure of GaAs

By definition, a crystal is any solid with an ordered arrangement of
its atoms. The cyrstal structure of GaAs can be thought of as a lattice
with repeated units of face-centered cubic (fcc) cells. Consider two types
of fcc cells, one with Ga atoms and another with As atoms. Imagine these
two fcc cells coalesced with the same origin at one corner. Now slide the
origin of the As cell along the vector $(a_o/4)[111]$ where a_o is the lattice

constant. The resulting fcc arsenic cell has its origin displaced to the point $\left(a_o/4, a_o/4, a_o/4\right)$ with respect to the gallium fcc origin. These interpenetrating fcc cells form a pattern which constitutes the GaAs lattice structure. The value of the lattice constant is $a_o = 0.56417$ nm.

SOS Model

The solid-on-solid (SOS) model is a square array of "blocks" stacked to form columns. This type of model can be represented by a square array of integers, where each integer represents the number of "blocks" in each column perpendicular to some reference plane. The "blocks" can represent atoms or molecules which are being stacked. Hereafter "blocks" will be referred to as adatoms. The SOS model is a generalization of the terrace-ledge-kink model (ref. 1), and the surface elements are those adatoms at the tops of their columns (see fig. 1). It is assumed that adatoms can be added (or removed) only to (from) positions over other solid adatoms.

In the SOS model the columns are built up upon an $M \times M$ square array by randomly placing adatoms upon the array and allowing these randomly deposited adatoms to either condense, evaporate, or migrate. The $M \times M$ array can be replaced by a single subscripted array so that only one random number is needed to select an arbitrary column (ref. 2). This one-to-one correspondence is illustrated in table 1. In the table, note that additional rows and columns have been added to the array. These augmented rows and columns will be used to eliminate edge effects and will be assigned periodic boundary conditions. We let $H(I)$ denote the height of a column at some arbitrary position I where $\eta + 1 \leq I \leq \eta + M^2$. The periodic boundary conditions imposed upon the heights are that they satisfy the conditions:

(1) Row 0 is the same as row M and
$$H(I) = H(I + M^2), \quad I = 10, \ldots, \eta + 1;$$

(2) Row 1 is the same as row M + 1 and
$$H(I) = H(I + M^2), \quad I + \eta, \ldots, \eta + M + 1; \text{ and}$$

(3) Column 0 is the same as column M and column 1 is the same as column M + 1 when the columns are displaced by one unit.
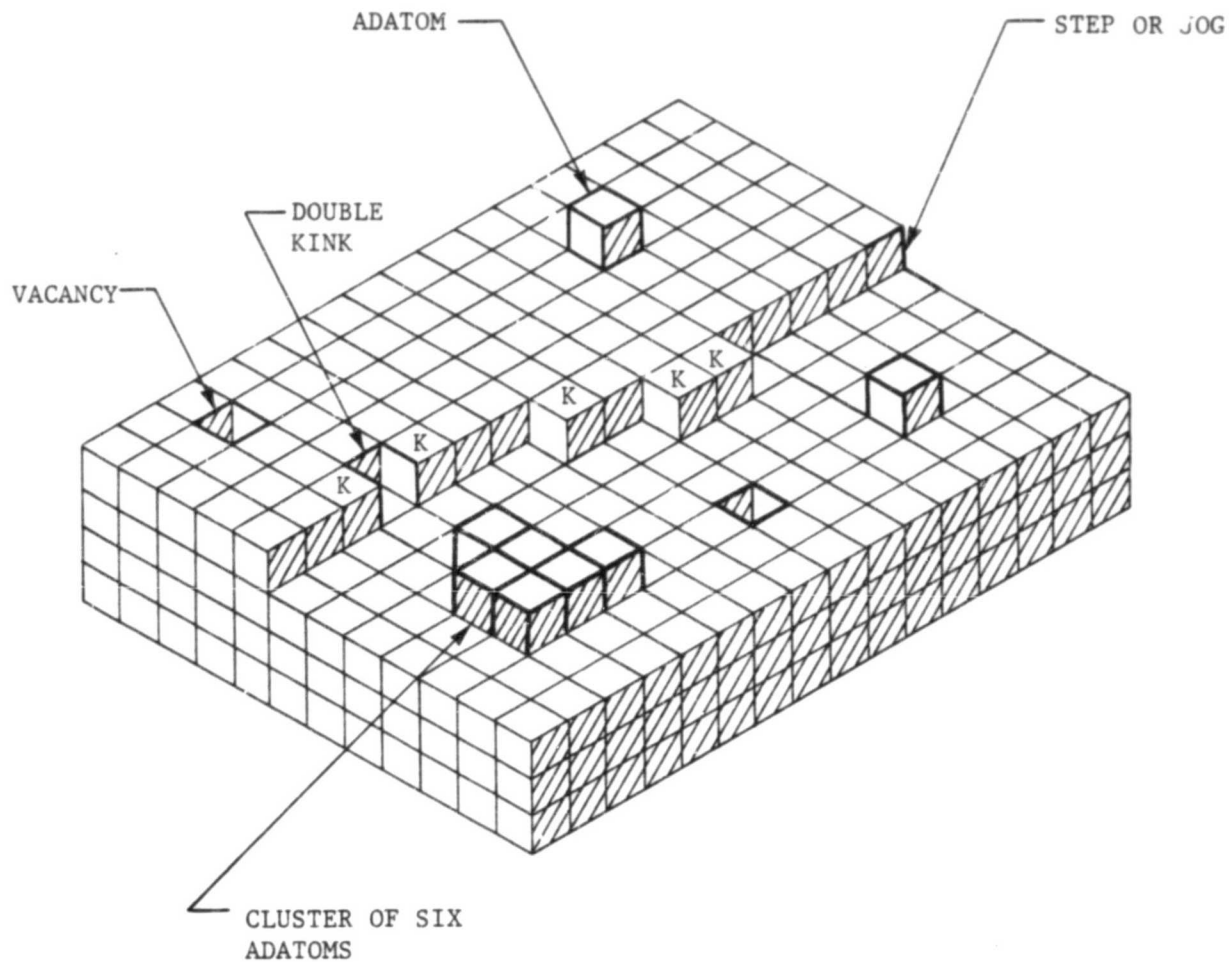
Figure 1. SOS model (K = kink site).

Table 1. Integers associated with row-column positions of M × M array ($\eta = 10 + M$).

Row Number	COLUMN NUMBER						
	0	1	2	...	M − 1	M	M + 1
0	10	10 + 1	10 + 2	...	$\eta - 1$	η	$\eta + 1$
1	η	$\eta + 1$	$\eta + 2$	...	$\eta + M - 1$	$\eta + M$	$\eta + M + 1$
2	$\eta + M$	$\eta + M + 1$	$\eta + M + 2$	...	$\eta + 2M - 1$	$\eta + 2M$	$\eta + 2M + 1$
3	$\eta + 2M$	$\eta + 2M + 1$	$\eta + 2M + 2$	...			
.							
.							
.							
M	$\eta + (M-1)M$	$\eta + (M-1)M + 1$	$\eta + (M-1)M + 2$	...	$\eta + M^2 - 1$	$\eta + M^2$	$\eta + M^2 + 1$
M + 1	$\eta + M^2$	$\eta + M^2 + 1$	$\eta + M^2 + 2$	...	$\eta + M^2 + M - 1$	$\eta + M^2 + M$	$\eta + M^2 + M + 1$

Thus, to each position I $(\eta + 1 \leq I \leq \eta + M^2)$, we can assign a height H(I) which represents the number of stacked adatoms. Also associated with a general position I there are neighboring positions which have the position indices given in table 2. The SOS model can be described as an array of interacting columns of varying integer heights. The surface adatoms are at the tops of columns.

The term "epitaxy" means "an arrangement on" and is used to denote the growth of one substance upon the crystal surface of a foreign substance. The term "auto-epitaxy" is the oriented growth of a substance onto itself, and "heteroepitaxy" is the growth over another material. Obviously, heteroepitaxy becomes autoepitaxy after one layer of growth has been deposited. We will use the SOS model to simulate epitaxial growth.

Potential Energy of Adatoms

The "rules" by which the columns of the SOS model interact will be governed by the following ideas relating to potential energy and the potential energy changes which are associated with the adsorption, migration or desorption of adatoms. We define the following energies:

$U_o = U_o(I)$ — potential energy at site I due to surface bonding and crystal structure

ϕ_o — potential energy change at site I due to the adsorption or desorption of adatoms (the same for all sites)

$-w_i (i=1,\ldots,8)$ — potential energy changes at neighboring sites when an adatom is deposited at I (the same for all sites)

$E(I)$ — random surface energy associated with site I and time interval Δt

$U(I) = U_o(I) + E(I)$ — total energy during time interval Δt.

U_e — evaporation potential

7

Table 2. Indices associated with neighbors surrounding a general position I within the M × M array of the SOS model.

I − M − 1	I − M	I − M + 1
I − 1	I	I + 1
I + M − 1	I + M	I + M + 1

U_m migration potential

All of the above energies are measured in electron volts.

We will develop a Monte Carlo computer simulation of crystal growth (refs. 3-8) by developing "rules" which determine the SOS kinetics of condensation, evaporation, or surface migration of adatoms. Consider first the adsorption of an adatom onto the surface at some general site I. In addition to the change in the potential at I, potential energy changes simultaneously occur at the sites neighboring the central site I. The potential energy changes are depicted by the mnemonic "mask" of table 3 which can be placed over the central site I to illustrate what changes must be made in the surrounding potential wells. We consider next the desorption of an adatom from the surface. In this case the potential energies at I and its neighboring sites again change and we use the mask of table 3 with opposite signs on the potential changes.

The case of surface migration is treated as a desorption from a site I followed by an adsorption at a nearest neighbor site to I together with the correct potential mask changes associated with each process. A random walk is performed to determine nearest neighbor migration sites.

The Monte Carlo simulation of crystal growth involves a random deposition of thermally accommodated surface adatoms during a time interval Δt. These deposited adatoms will change the potential energies at the surface sites under consideration. The values assigned to ϕ_o and $-\omega_i, i=1,\ldots,8$ will dictate the changes in potential energies. We assume that the surface adatoms have a known a priori surface energy distribution $f(E)$ from which we can assign random energies to the surface adatoms. We let

$$U(I) = U_o(I) + E(I) \tag{1}$$

denote the total energy assigned to a surface adatom during the time interval Δt. This total energy is the sum of the potential energy $U_o(I)$ due to the structure of the lattice and the random energy $E(I)$ from the assumed surface energy distribution $f(E)$. If $U(I)$ is less than some material-

Table 3. Potential energy adjustments associated
with each site I.

$-\omega_7$	$-\omega_8$	$-\omega_1$
$-\omega_6$	ϕ_0	$-\omega_2$
$-\omega_5$	$-\omega_4$	$-\omega_3$

dependent migration level U_m, then the adatom will remain at the site I. If $U(I)$ is greater than some material-dependent evaporation level U_e, then the adatom will evaporate from the surface. For $U_m < U < U_e$, then surface migration is allowed to occur. During each time interval Δt there is a random deposition of adatoms upon the surface. Each of these new adatoms together with the other surface adatoms is assigned a random energy and tested to determine if it remains on the surface, migrates, or evaporates from the surface.

This type of model can simulate the atomic or molecular exchange between vapor and solid phases of crystal growth. We assume that an adatom is a two-component species of Ga and As. Also, in the Monte Carlo simulation, it is assumed that the rate of impingement of adatoms is independent of the neighboring surface configurations. The number of thermally accommodated adatoms which arrive on the surface is given by

$$\nu_{io} = \frac{P}{(2\pi mKT)^{\frac{1}{2}}} \qquad (2)$$

where P is the vapor pressure, M is the vapor adatom mass, K is Boltzmann's constant, and T is the absolute temperature.

The rates associated with evaporation and migration of adatoms depend upon the neighboring potentials which must be broken during these processes and also upon the random surface energy distribution which is assumed. The fate of a surface adatom depends upon its total energy U at any instant of time as well as upon where this energy lies with respect to the condensation and evaporation energy levels U_m and U_e.

In assuming values to the potential changes ϕ_o and $\omega_i, i=1,\ldots,8$, we must take into account the type of crystal structure and orientation we are trying to simulate with our SOS model. Consider figure 2 which illustrates the GaAs fcc structure. For growth on the (100) face we can set up a correspondence between a central site, the nearest neighbor sites, second nearest neighbor sites, and the adatom potential changes for the mask in table 3 (i.e., $\omega_1 = \phi_2$, $\omega_2 = \phi_1$, etc.). Similarly, we can set up the correspondences illustrated in figures 2 (b and c) for the (111) and (110) orientations.

In figure 2 we must choose $\phi_0, \phi_1, \phi_2, \phi_3$ in such a way that, when the first level of adatoms covers the surface, then the potential distribution must return to its original value. We will require that adjustments be made in the potential energy changes during the transition from heteroepitaxy to autoepitaxy. Here we let a negative sign denote an attractive potential. By simply adding adatoms to a surface it is readily verified that the potential changes must adhere to the rules given in table 4 if after one layer the potential energy returns to its initial value.
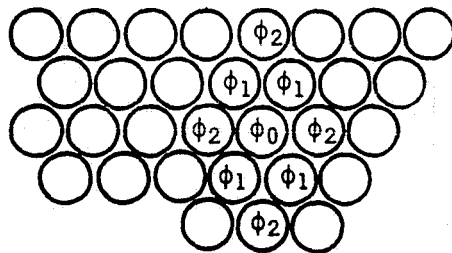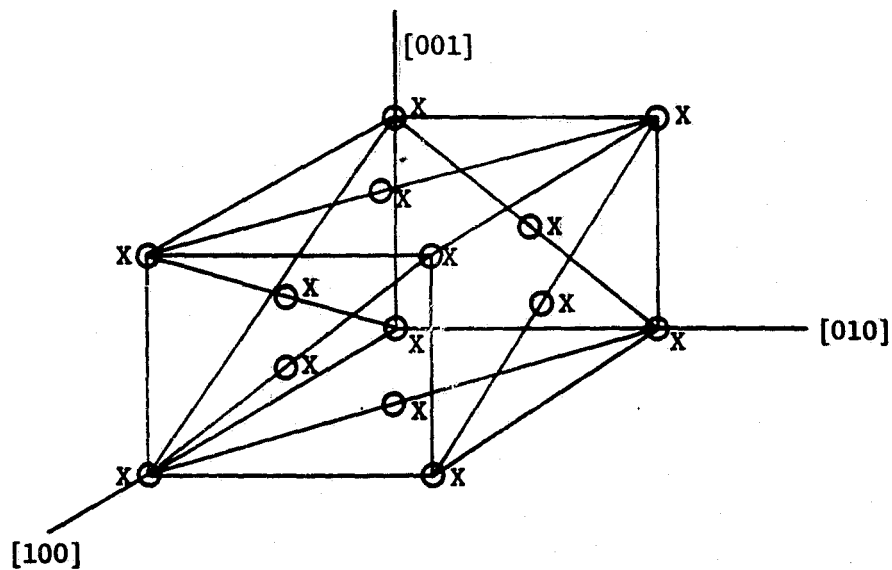
We can assign arbitrary values to the neighbor potential changes ϕ_1, ϕ_2, ϕ_3 or we can assume a (m_o, n_o) Mie potential, with $m_o < n_o$, (ref. 9):

$$\phi = \phi^* \left[\left(\frac{R^*}{R} \right)^{n_o} - \frac{n_o}{m_o} \left(\frac{R^*}{R} \right)^{m_o} \right] \tag{3}$$

which is illustrated in figure 3. Here R^* is the distance at which ϕ obtains its minimum value of $\phi^* \left(1 - \frac{n_o}{m_o} \right)$. Table 5 gives values of ϕ/ϕ^* for various R^*/R values.

The values assigned to the mask potential changes are not necessarily the same for the different orientations: for example, the ϕ_1, ϕ_2, ϕ_3 values for each case in table 4 could have different values.

If we assume a $(3,9)$ Mie potential and an fcc crystal, we can calculate the potential changes caused by adding adatoms to neighboring sites. If we leave the central position empty and fill nearest neighbor sites first, then second nearest neighbor sites, followed by adatoms to third nearest neighbor sites, and then fill in the central position, we will obtain the curves in figure 4. In figure 4 the lower curves are when the site I is initially empty and the upper curves are for the site I initially occupied by an adatom. An examination of figure 4 shows that, if we add a random energy to the curves illustrated, then the upper curves represent the potential energies associated with groups of adatoms clustering about I. If we consider a cluster of adatoms which is smaller than some critical cluster size, then this cluster will be unstable in the sense that an adatom at site I will
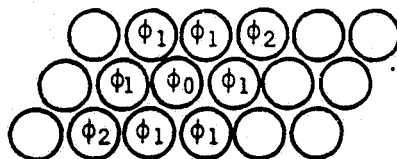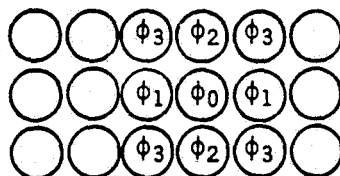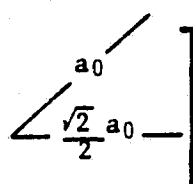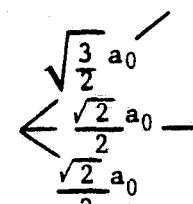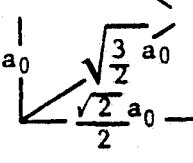
Figure 2. GaAs cell with growth patterns and potential changes for (100), (111), and (110) faces.

13

Table 4. Potential changes for addition of an adatom to an arbitrary site.

Crystal Face	Relation Between Neighbor Potentials	Potential Changes For Addition to Arbitrary Site I	Distances to Neighboring Sites
		$$\begin{bmatrix} -\omega_7 & -\omega_8 & -\omega_1 \\ -\omega_6 & \phi_0 & -\omega_2 \\ -\omega_5 & -\omega_4 & -\omega_3 \end{bmatrix}$$	
100	$\phi_0 = 4\phi_1 + 4\phi_2$	$$\begin{bmatrix} -\phi_2 & -\phi_1 & -\phi_2 \\ -\phi_1 & \phi_0 & -\phi_1 \\ -\phi_2 & -\phi_1 & -\phi_2 \end{bmatrix}$$	$\begin{bmatrix} a_0 \\ \dfrac{\sqrt{2}}{2}a_0 \end{bmatrix}$
111	$\phi_0 = 6\phi_1 + 2\phi_2$	$$\begin{bmatrix} -\phi_1 & -\phi_1 & -\phi_2 \\ -\phi_1 & \phi_0 & -\phi_1 \\ -\phi_2 & -\phi_1 & -\phi_1 \end{bmatrix}$$	$\begin{bmatrix} \sqrt{\dfrac{3}{2}}a_0 \\ \dfrac{\sqrt{2}}{2}a_0 \\ \dfrac{\sqrt{2}}{2}a_0 \end{bmatrix}$
110	$\phi_0 = 2\phi_1 + 2\phi_2 + 4\phi_3$	$$\begin{bmatrix} -\phi_3 & -\phi_2 & -\phi_3 \\ -\phi_1 & \phi_0 & -\phi_1 \\ -\phi_3 & -\phi_2 & -\phi_3 \end{bmatrix}$$	$\begin{bmatrix} a_0 & \sqrt{\dfrac{3}{2}}a_0 \\ & \dfrac{\sqrt{2}}{2}a_0 \end{bmatrix}$
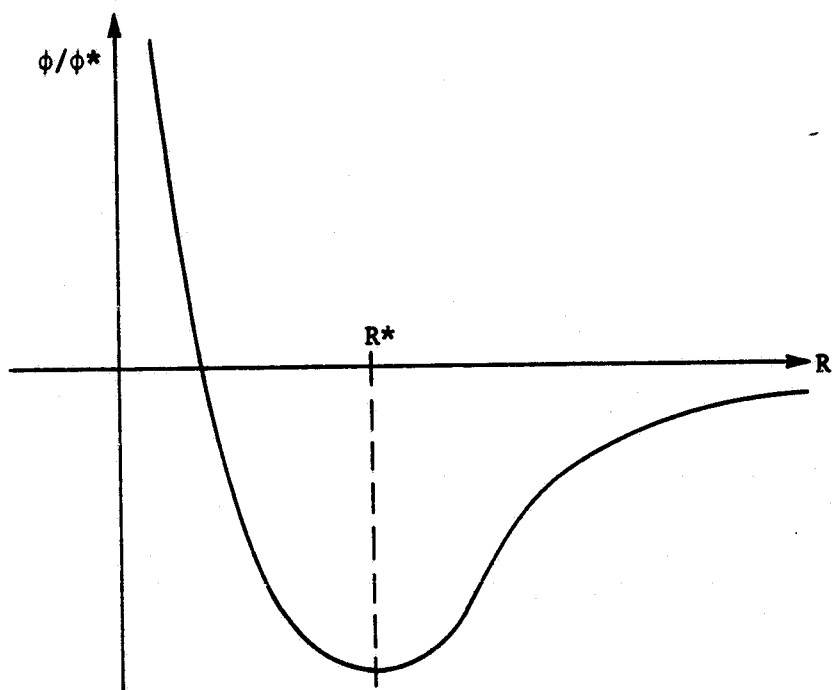
Figure 3. (n_o, m_o) Mie potential function.

Table 5. Mie potentials.

m	n	ϕ/ϕ^*		
		$R^*/R = 1$	$R^*/R = 1/2$	$R^*/R = 1/3$
3	6	-1	-0.582	-0.348
3	7	-1.333	-0.736	-0.428
3	8	-1.666	-0.880	-0.500
3	9	-2	-1.016	-0.570
4	7	-0.75	-0.349	-0.173
4	8	-1	-0.437	-0.210
4	9	-1.25	-0.518	-0.242
4	10	-1.5	-0.594	-0.273
4	11	-1.75	-0.665	-0.303
4	12	-2.0	-0.734	-0.332
5	8	-0.6	-0.220	-0.090
5	9	-0.8	-0.274	-0.108
5	10	-1.0	-0.322	-0.124
5	11	-1.2	-0.366	-0.138
6	9	-0.5	-0.143	-0.048
6	10	-0.666	-0.177	-0.058
6	11	-0.833	-0.207	-0.065
6	12	-1.0	-0.234	-0.073
7	11	-0.57	-0.116	-0.031
7	12	-0.714	-0.135	-0.035

Figure 4. Change in potential energy at site I due to deposition of adatoms to neighboring sites (nearest neighbors filled first with assumed (3,9) Mie potential).

have a probability of greater than 1/2 of leaving the cluster. In the case where the cluster size is greater than the critical cluster size, then we desire such a cluster to be stable in the sense that an adatom at site I will have a probability of less than one-half of leaving the cluster.

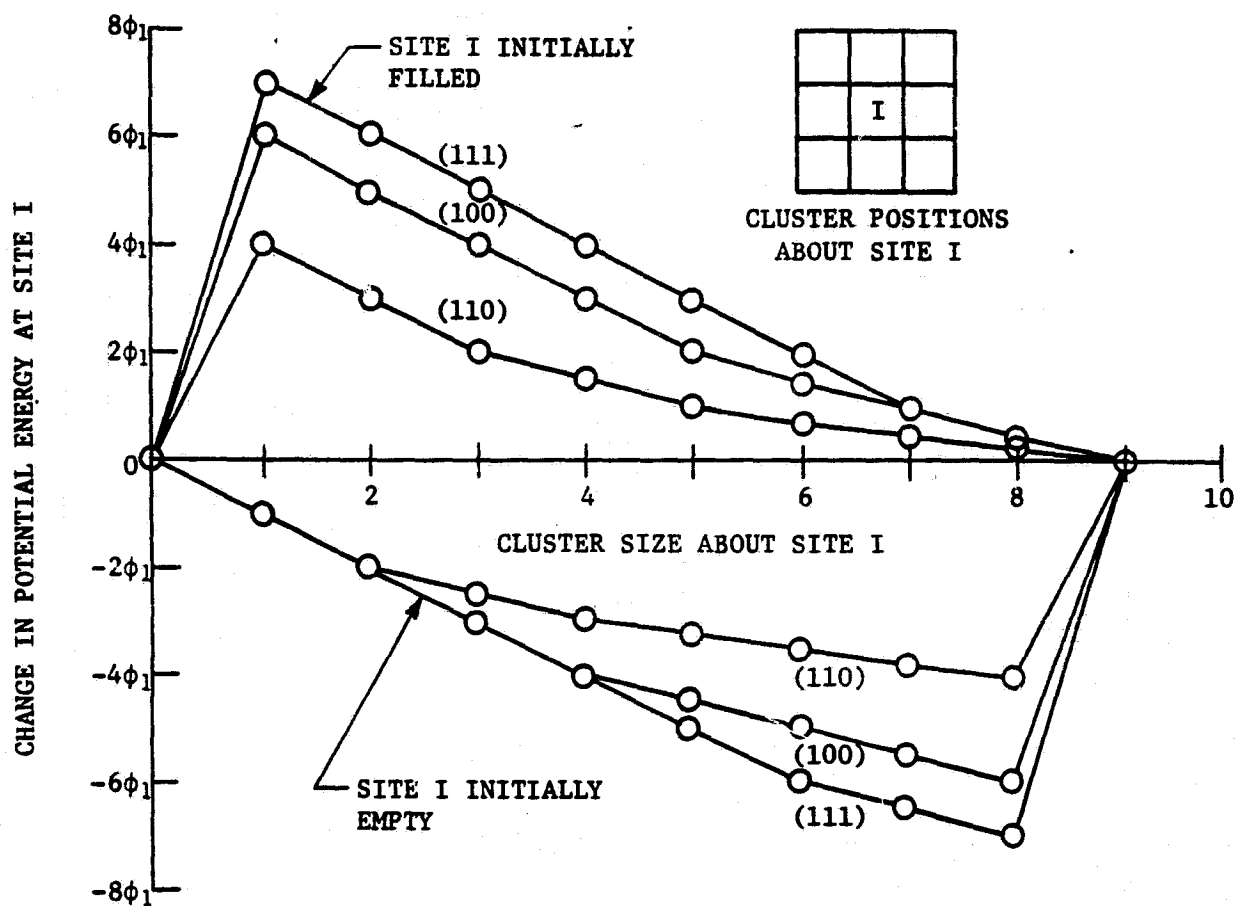For a (m_o, n_o) Mie potential, we can express the second and third nearest neighbor potentials ϕ_2, ϕ_3 in terms of the nearest neighbor potential ϕ_1, and we can write

$$\phi_2 = \alpha_2 \phi_1$$

$$\phi_3 = \alpha_3 \phi_1$$

(4)

where α_2, α_3 are appropriate scale factors (see, for example, table 5). Using the potential masks of table 4, we can calculate the potential energies at an arbitrary site I for different crystal orientations and various cluster sizes about the central site. These various potentials are given in table 6 for arbitrary $U_o, \alpha_2, \alpha_3, \phi_1$ values.

In our computer model we will assign a value to ϕ_o, the potential change due to the addition of an adatom at site I. Then from the (m_o, n_o) Mie potential and the relations $\phi_o = 4\phi_1 + 4\phi_2 = (4 + 4\alpha_2)\phi_1$ (100 case), $\phi_o = 6\phi_1 + 2\phi_2 = (6 + 2\alpha_2)\phi_1$ (111 case) and $\phi_o = 2\phi_1 + 2\phi_2 + 4\phi_3 = (2 + 2\alpha_2 + 4\alpha_3)\phi_1$ (110 case), we can determine the nearest neighbor potential change ϕ_1 and from equation (4) the other potential changes for nonnearest neighbors. In our model we will use a (4,10) Mie potential (refs. 9, 10).

The data presented in figure 4 and table 5 can be used to make a rough limited estimate of the nearest neighbor potential ϕ_1 in the following sense: we assume that the surface thermodynamics can be attributed to the property of clusters. Using the Gibb's free energy of formation of a spherical cluster of radius r as

$$\Delta G = 4\pi r^2 \sigma - \frac{4}{3}\pi r^3 \frac{KT}{V} \ln \frac{P}{P_e}$$

where r = radius of cluster, σ = surface vapor interface energy, V = molecular volume, T = absolute temperature, P = supersaturated vapor pressure, P_e = equilibrium pressure (P/P_e = supersaturation). (See figure 5 for a diagram of potential energy.) Here ΔG is a maximum at

$$r = r^* = \frac{2\sigma V}{KT \ln \frac{P}{P_e}}$$

This is the radius of the critical cluster. If a cluster has a radius r which is smaller than r^*, then the cluster will be unstable and an adatom will have a probability of greater than one-half of leaving the cluster. Alternatively, if the radius of the cluster is larger than r^*, then an adatom will have a probability of less than one-half of leaving the cluster.

These ideas can be incorporated into our model in a limited sense as follows: We let $U_e = 0$ denote the evaporation level; and ΔU_e then represents the desorption energy of a surface adatom and $\Delta_e = U_e - U_o$ or $U_o = -\Delta U_e$, for ΔU_m, the activation energy for migration, we have $U_m - U_o = \Delta U_m$. By using the results of table 6, other potential energies can be visualized inside the potential well. Usually, $\Delta U_e, \Delta U_m$ are measured at reference T_r, and it will be assumed that these values are temperature independent. We also assume that the thermally accommodated adatoms have a Boltzmann distribution which has the median value $E_{median} = KT_r \ln 2$, where K is Boltzmann's constant. If we assume a critical cluster size and choose ϕ_o such that this cluster has an equal probability of growing larger or smaller, we have for the different crystal orientations the requirement that, when a median energy from the Boltzmann distribution is added to the energy of an adatom associated with a critical cluster, we obtain

$$\underbrace{U_o + g_n \phi_1}_{\substack{\text{energy of critical} \\ \text{cluster adatom}}} + \underbrace{KT_r \ln 2}_{\substack{\text{median} \\ \text{energy}}} = \underbrace{U_m}_{\substack{\text{migration} \\ \text{energy}}} \qquad (5)$$

Equation (5) enables us to determine ϕ_1 such that 50 percent of the adatoms will remain at the site I, while 50 percent of the adatoms will desorb from the site I. An example which will illustrate the use of equation (5) is given in the next section. Also, the limitations of using equation (5) to assign a value to ϕ_1 will be discussed.
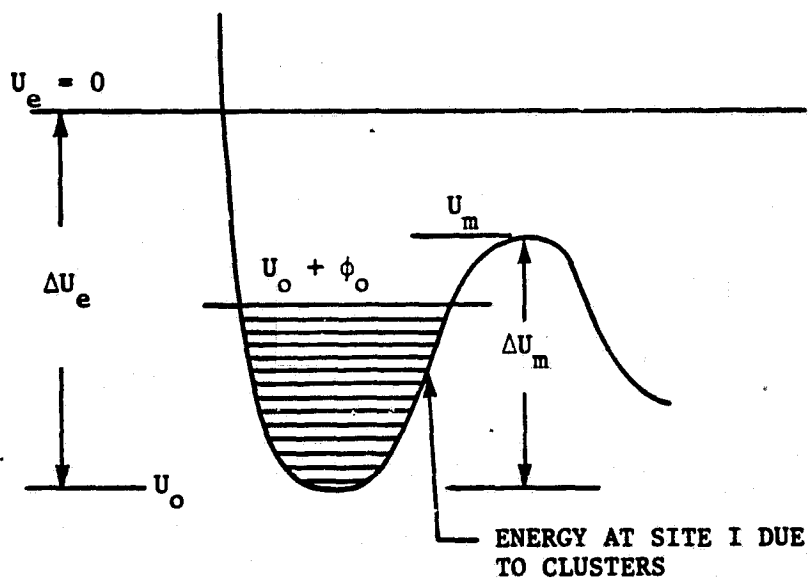
Figure 5. Potential energy.

Table 6. Potential energies at arbitrary site I.

Cluster Size n	Potential at Site I $U_o + g_n\phi_1$		
	100	111	110
0	U_o	U_o	U_o
1	$U_o + (4 + 4\alpha_2)\phi_1$	$U_o + (6 + 2\alpha_2)\phi_1$	$U_o + (2 + 2\alpha_2 + 4\alpha_3)\phi_1$
2	$U_o + (3 + 4\alpha_2)\phi_1$	$U_o + (5 + 2\alpha_2)\phi_1$	$U_o + (1 + 2\alpha_2 + 4\alpha_3)\phi_1$
3	$U_o + (2 + 4\alpha_2)\phi_1$	$U_o + (4 + 2\alpha_2)\phi_1$	$U_o + (2\alpha_2 + 4\alpha_3)\phi_1$
4	$U_o + (1 + 4\alpha_2)\phi_1$	$U_o + (3 + 2\alpha_2)\phi_1$	$U_o + (\alpha_2 + 4\alpha_3)\phi_1$
5	$U_o + 4\alpha_2\phi_1$	$U_o + (2 + 2\alpha_2)\phi_1$	$U_o + 4\alpha_3\phi_1$
6	$U_o + 3\alpha_2\phi_1$	$U_o + (1 + 2\alpha_2)\phi_1$	$U_o + 3\alpha_3\phi_1$
7	$U_o + 2\alpha_2\phi_1$	$U_o + 2\alpha_2\phi_1$	$U_o + 2\alpha_3\phi_1$
8	$U_o + \alpha_2\phi_1$	$U_o + \alpha_2\phi_1$	$U_o + \alpha_3\phi_1$
9	U_o	U_o	U_o

Energy Distribution and Random Walk

In our model of crystal growth we assume that the thermally accommo-
dated adatoms possess a Boltzmann distribution for their surface energies.
This distribution can be expressed as

$$f(E) = \frac{1}{KT} \exp\left(-\frac{E}{KT}\right) \qquad (6)$$

It has the cumulative distribution function:

$$F(E) = \int_0^E f(E)dE = 1 - \exp\left(-\frac{E}{KT}\right) \qquad (7)$$

We can generate a random variate E from this Boltzmann distribution by
using the inverse function associated with the cumulative distribution [eq.
(7)]. For R, a uniform random number between 0 and 1, the random energy is
given by

$$E = -KT \ln (1 - R) \qquad (8)$$

The mean of this distribution is KT and the median is given by

$$E_{median} = KT \ln 2 \qquad (9)$$

We will choose the nearest neighbor potential ϕ_1 by assuming a criti-
cal cluster size (refs. 11, 12) from table 6. For example, if we choose 3
as the critical cluster size, then we desire that an adatom added to site I
will have a probability of less than one-half of leaving the cluster. For a
(100) orientation, we require that

$$U_{3CLUSTER}(100) + E_{median} = U_m$$

or

$$U_0 + (2 + 4\alpha_2) \phi_1 + KT_r \ln 2 = U_m$$

This requires that we choose ϕ_1 to satisfy

$$\phi_1 = \frac{U_m - U_o = KTr \ln 2}{(2 + 4\alpha_2)} = \frac{\Delta U_m - KTr \ln 2}{(2 + 4\alpha_2)} \qquad (10)$$

where ΔU_m is the surface diffusion activation energy. For this choice of ϕ_1 we will then have the following inequalities:

for cluster sizes greater than three,

$$U_{nCLUSTER}(100) + E_{median} < U_m, \quad n > 3$$

for cluster sizes less than three,

$$U_{nCLUSTER}(100) + E_{median} > U_m, \quad n < 3$$

The appropriate choice of U_m then produces the stability and instability characteristics associated with various size clusters.

In general, we can replace the denominator in equation (10) by the more-general expression $g_n = (n_1 + m_1\alpha_1 + \ell_1\alpha_2)$ where n_1, m_1, ℓ_1 are integers associated with different crystal orientations. This produces the more general expression

$$\phi_1 = \frac{\Delta U_m - KT_r \ln 2}{g_n} \qquad (11)$$

For the nearest neighbor potential c nge associated with a g_n critical cluster and surface orientation of table 6. In equation (11) the Mie potential is assumed, and second, third nearest neighbors' potential changes are given by

$$\phi_2 = \alpha_2\phi_1, \quad \phi_3 = \alpha_3\phi_1$$

and T_r is a reference temperature.

We can thus summarize the Monte Carlo simulation model as follows:

(1) We assign an initial geometry and characteristics to a sub-
strate. In addition to geometry considerations, we assign a

uniform potential (U_{os}) together with evaporation (U_{es}) and migration (U_{ms}) levels.

(2) Heteroepitaxy is assumed to occur during deposition of the first layer. A flat uniform surface would have potential changes from a uniform value of U_{os} everywhere on the substrate to a value of U_o everywhere after the first layer covers the substrate. Because of this change from heteropitaxy to autoepitaxy, the initial layer potential mask is adjusted by a value of $U_o - U_{os}$, from which we can obtain the heteroepitaxy-to-autoepitaxy potential change.

(3) We assume Mie potentials for both the substrate and growing material. The nearest neighbor potential change ϕ_1 is determined by $\Delta U_D = U_m - U_o$, which is the surface diffusion activation energy, temperature, critical cluster size, and surface orientation. The second and third nearest neighbor potential changes ϕ_2, ϕ_3 are determined by the Mie potential scale factors α_2, α_3, and $\phi_2 = \alpha_2\phi_1$, $\phi_3 = \alpha_3\phi_1$ we can then construct the appropriate potential masks depicted in table 4 for both the substrate and the growing materials.

(4) During a time interval Δt we let adatoms impinge upon the surface and update the potentials U_o.

(5) During the Δt interval, each of the surface adatoms is assigned a random energy (E) from a Boltzmann distribution and the total energy at each adatom surface site is tested. For $U = U_o + E$, the total energy, we let the adatom:

evaporate if $U > U_e$;

migrate if $U_m < U < U_e$; and

remain stationary if $U < U_m$.

During the heteroepitaxy, we use the values U_{es}, U_{ms} to determine the fate of an adatom, and for autoepitaxy we use the values U_e and U_m.

(6) We record and update all potential changes and height changes which occur during the growth process together with other sta-

24

tistical measures of crystal growth to which we may want to assign a quantitative value.

(7) The process continues until some stopping condition is satisfied. Some stopping conditions are that (a) layers exceed a certain value or (b) time exceeds a certain value.

During the surface migration of an adatom, we allow it to random walk to a nearest neighbor site only. Only those nearest neighbor sites which are unoccupied and at the same or a lower level are considered first for the random walk. If all the nearest neighbor sites on the same level are filled, then the adatom is allowed to random walk to a nearest neighbor site by hopping up to the next highest level. The flow chart of the computer simulation is illustrated in figure 6.

The limitations in calculating ϕ_1, rather than assigning a value to ϕ_o (which is more general), are as follows: let $C_o = KT_r \ln 2$, then from equation (11) we can construct the following linear relation $\phi_o = m(\Delta U_m - C_o)$ where the values of the slope m are given for different cases:

Critical Cluster Size	Orientation		
	100	111	110
2	$m = \dfrac{4(1 + \alpha_2)}{3 + 4\alpha_2}$	$m = \dfrac{(6 + 2\alpha_2)}{5 + 2\alpha_2}$	$m = \dfrac{(2 + 2\alpha_2 + 4\alpha_3)}{1 + 2\alpha_2 + 4\alpha_3}$
3	$m = \dfrac{4(1 + \alpha_2)}{2 + 4\alpha_2}$	$m = \dfrac{(6 + 2\alpha_2)}{4 + 2\alpha_2}$	$m = \dfrac{(2 + 2\alpha_2 + 4\alpha_3)}{2\alpha_2 + 4\alpha_3}$
4	$m = \dfrac{4(1 + \alpha_2)}{1 + 4\alpha_2}$	$m = \dfrac{6 + 2\alpha_2}{3 + 2\alpha_2}$	$m = \dfrac{(2 + 2\alpha_2 + 4\alpha_3)}{\alpha_2 + 4\alpha_3}$

$$(12)$$

These relations imply that for ΔU_m large enough, $U_o + \phi_o > 0$; consequently these adatoms will evaporate from the surface. Clearly, we do not want ϕ_o to be dependent upon the choice of ΔU_m. As a consequence, the cluster interpretation still exists, yet we must assign a value to ϕ_o which is independent of ΔU_m.

READ IN VALUE OF PARAMETERS

INITIALIZATION OF SUBSTRATE
GEOMETRY AND POTENTIALS

IMPINGEMENT OF L RANDOM
ADATOMS DURING TIME INTERVAL Δt

UNIFORM DISTRIBUTION: GENERATE L
RANDOM SITES AND DEPOSIT ADATOMS AT THESE
SITES AND CHANGE POTENTIALS BY USING
APPROPRIATE MASK

DO FOR ALL SURFACE ADATOMS (SITE I)

BOLTZMAN DISTRIBUTION: GENERATE RANDOM
SURFACE ENERGY E(I)

TEST POTENTIAL AT SITE I, $U = U_0(I) + E(I)$

IF $U \leq U_m$ THEN ADATOM REMAINS AT SITE

IF $U \geq U_e$ THEN EVAPORATION FROM SITE

IF $U_m < U < U_e$ THEN MIGRATION TO NEW SITE

CONDENSATION: LEAVE ADATOM
AT SITE I

MIGRATION: RANDOM WALK FROM
SITE I TO NEAREST NEIGHBOR SITE
UPDATE POTENTIALS BY EVAPORATING
ADATOM FROM I AND DEPOSITING
ADATOM AT NNS.

EVAPORATION: ADATOM REMOVED
FROM SURFACE AND POTENTIALS
UPDATED

CONTINUE

CALCULATE: STATISTICAL AVERAGES OF VARIOUS
"MEASURES" OF CRYSTAL GROWTH - OUTPUT DATA
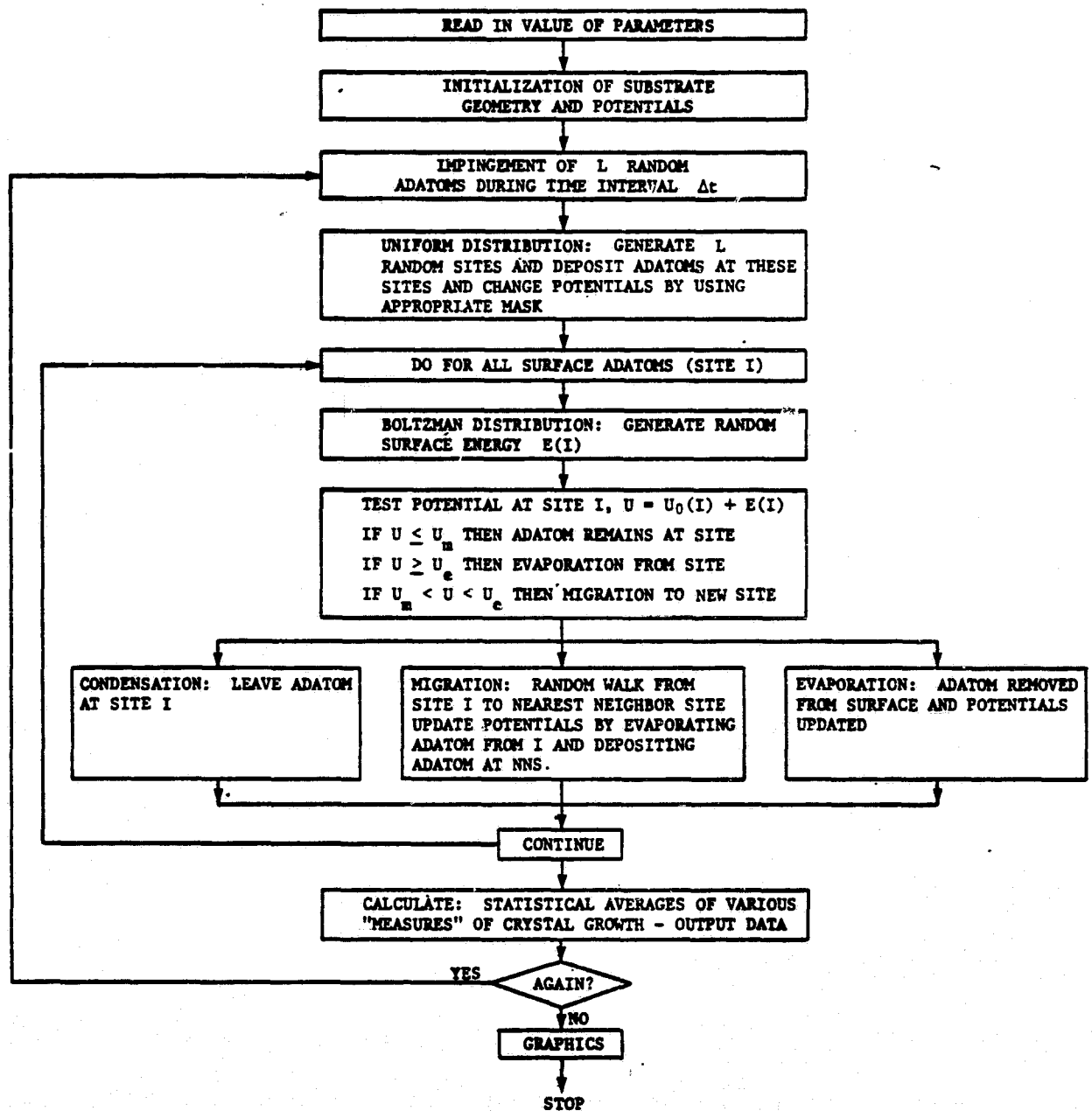
YES   AGAIN?   NO

GRAPHICS

STOP

Figure 6.   Flow chart of model.

ADDITIONAL CONSIDERATIONS AND ASSUMPTIONS

With reference to figure 7, we have the following situation: When material is deposited upon an ideally flat substrate, the potential wells will change from U_{os} to U_o after one layer of material covers the substrate. In order to accomplish this change, we alter the potential mask of table 4 by replacing ϕ_o by $\phi_o + U_o - U_{os}$ for all first-layer locations. For layers greater than one, we revert back to the masks of table 4.

The interatomic potential possesses the general characteristics of figure 7. If we assume that $R_1^* = R_2^* = a_o$ is the interatomic spacing, then the first-layer potential adjustment will be $U_o - U_{os}$ as above. If, however, there is a misfit dislocation in the atomic spacing of the substrate and deposited material, then the first-layer potential adjustment will be in terms of the different potentials at R_1^* and R_2^* and will vary accordingly upon the misfit distance. The first-layer potential adjustments will, in general, have to be corrected as we move along the misfit direction as suggested by figure 8. This will require much additional bookkeeping of potential values and changes with distance.

Imagine that we move an adatom along the flat surface. For each displacement S, measured from some fixed reference, the adatom will experience a potential attraction or repulsion which is determined by the Mie potential. For each value of $S = 0, a_1, 2a_1, \ldots$, there will be an associated potential change which can be calculated for each position. This would require that the potential masks of the first layer would each have to be adjusted based upon the assumed geometry and calculated Mie potential values.

For a heterogeneous surface, the evaporation potential changes will vary from site to site as will the nearest neighbor migration levels. If we let U_{ij} denote the potential well at a position i,j and denote by ΔU_e the average evaporation energy, and ΔU_m the average migration energy, then associated with each site potential $U_{i,j}$ there are nearest neighbor migration levels $\Delta U_{m,1}, \Delta U_{m,2}, \ldots$ in each of the nearest neighbor directions, as illustrated in figure 9. These additional concepts will require a more detailed computer model to keep track of all the potential changes and updates.
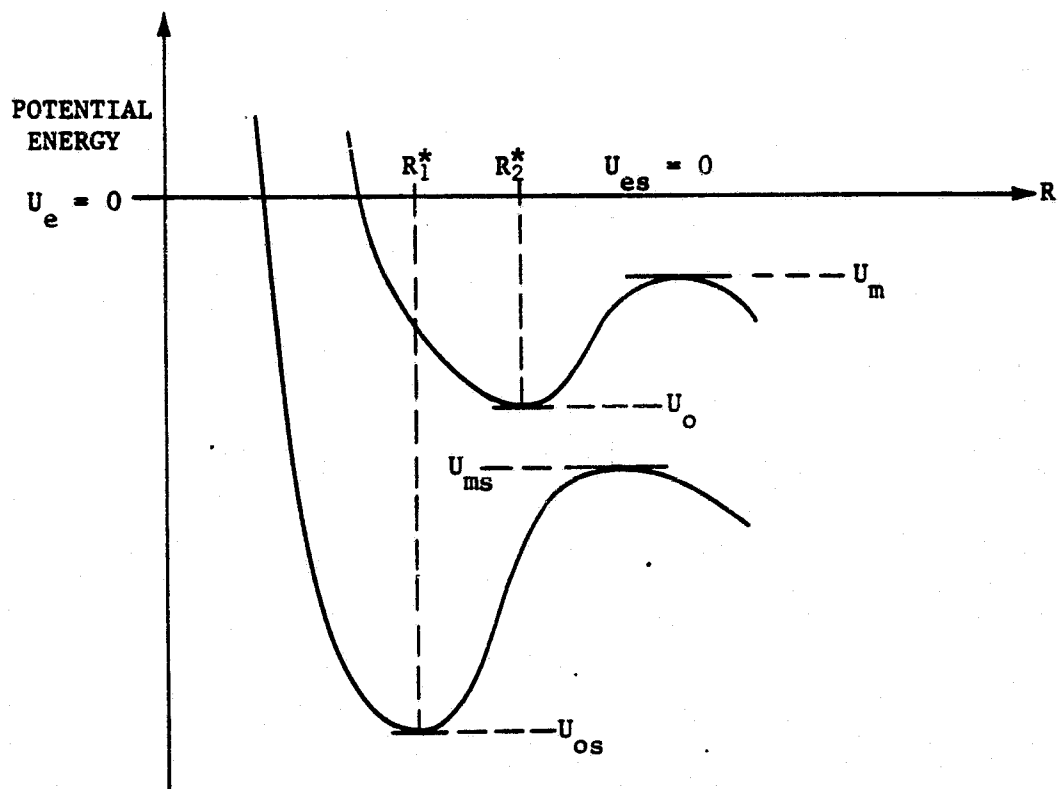
Figure 7. Potential energy diagrams for growing material and substrate.
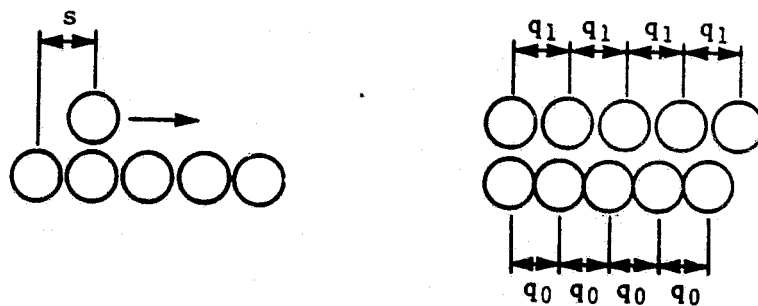
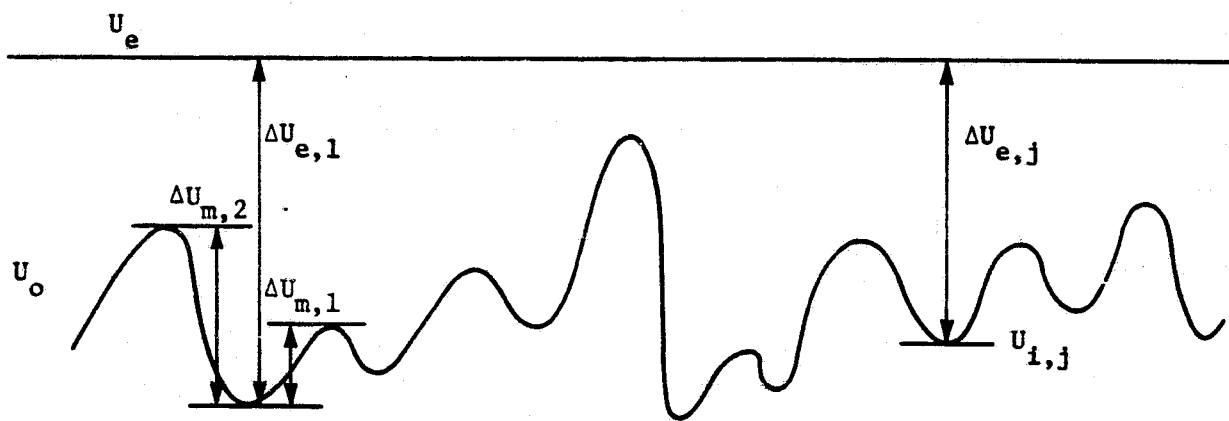Figure 8. Misfit dislocation approximation.

Figure 9. Heterogeneous surface potentials.

We begin our study with the oversimplified model flow charted in figure 6 where we assume a (4,10) Mie potential and let the critical cluster size determine ϕ_1 and consequently ϕ_0. For future studies we will assign values to ϕ_0 independent of ΔU_m values and try to determine the feasibility of extending the concepts to an A-B model. The following section summarizes the processes which the model considers.

SUMMARY AND DESCRIPTION OF GROWTH PROCESS

We simulate the number of adatoms impinging upon an area of the substrate during a time interval Δt. These adatoms impinge at random positions on the surface and will be absorbed, migrate, or desorb depending upon their energy states during the time interval Δt. The deposited adatoms will form clusters (refs. 10, 13). The sizes and shapes of these clusters will be determined by the energies of the potential wells, the deposition rates, the migration levels, and the surface temperature which affect the surface energy Boltzmann distribution.

When conditions are such that surface diffusion controls the growth, the clusters that form will increase in size and eventually coalesce with other clusters. After the clusters coalesce, the islands of clusters will have empty spaces between them which will fill in and disappear by the random deposition of adatoms.

The surface energy is an important mechanism which controls the surface diffusion and mass transport of surface adatoms since this diffusion process enables clusters to form, then grow and finally merge with other clusters. We assume that thermally accommodated adatoms are described by a Boltzmann distribution

$$f(E) = \frac{1}{KT} \exp\left(\frac{-E}{KT}\right) \quad , \quad E > 0 \tag{13}$$

which has a mean $\overline{E} = KT$, mode of $E_{mode} = 0$, and median of $E_{median} = KT \ln 2$.

Note that for τ_s, the average lifetime of a monomer adatom on the surface before it desorbs from the surface, we may write

$$\tau_s = \frac{1}{\upsilon_1} \exp \frac{\Delta U_e}{KT} \qquad (14)$$

where ΔU_e is the evaporation energy from the surface to the vapor and υ_1 is a frequency factor on the order of 10^{-12} to 10^{-13} seconds at room temperature. Letting D_s denote the monomer diffusion coefficient we write

$$D_s = d_o^2 \upsilon_o \exp \frac{\Delta U_m}{KT} \qquad (15)$$

where ΔU_m is the activation energy necessary for an adatom to jump a lattice distance d_o to a neighboring site and υ_o is the frequency factor for the jump. For diffusion-dominated phenomena, the adatoms form clusters by way of collisions on the surface. The value of ΔU_m depends upon where the monomer is located (i.e. kink site, edge, free adatom, etc.). We will assume that ΔU_m is associated with a kink site energy change. From the Einstein relation

$$D_s \tau_s = X_s^2 \qquad (16)$$

where X_s is the mean adatom displacement, we can write

$$X_s = d_o \sqrt{\frac{\upsilon_o}{\upsilon_1}} \exp \left(\frac{\Delta U_e - \Delta U_m}{2KT} \right) \qquad (17)$$

Now if diffusion is the dominant mechanism for growth, then $X_s > d_o$ and we require that $\Delta U_e > \Delta U_m$.

Also associated with the growth mechanism are the deposition rate and migration range and how these quantities interact. For example, with a low deposition rate and large values for ΔU_e and small ΔU_m there will be a high probability for surface migration of adatoms deposited. This surface diffusion is a random walk process which continues until the adatom is absorbed by the surface or else desorbs back to the vapor. At the other extreme, if the deposition rate is much greater than the diffusion rate, then the adatoms are being deposited before other adatoms can migrate away by surface diffusion. The large deposition rate creates the interaction of adatoms and the resultant cluster formation.

The size of the crystal formed will depend upon:

(1) the surface mobility of the adatoms;

(2) the smoothness of the substrate as a growing surface (i.e., the rougher the surface, the more nucleation sites available and the higher the probability of anisotropic column growth. Also, there will be a reduced surface mobility of adatoms);

(3) the deposition rate and the kinetic theory of interaction and chemical bonding of adatoms on the surface which will tend to increase the average energy of surface adatoms (i.e. for those substrates where there is a strong interaction between adatoms, then the adatom surface mobility will be reduced);

(4) the activation energies for surface diffusion and evaporation; and

(5) the orientation of the critical clusters and their density at the onset of nucleation.

If the surface energy distribution is such that at low temperatures the adatom surface migration is small, then the crystal growth is mainly from condensation on random surface sites. If R_d is the deposition rate and R_e the evaporation rate from a surface section which has M^2 adatoms and d_o is the depth of a layer, then

$$R_g = \frac{d_o (R_d - R_e)}{M^2} \tag{18}$$

is the average growth rate.

If the substrate material is amorphous in structure, then the potential wells will not be periodic in nature. This will decrease the surface mobility of adatoms and the impinging adatoms will tend to condense in the neighborhood of impingement.

The epitaxial relationship between the substrate material and the condensating material, in regards to preferential oriented absorption, depends upon the relative potential wells and consequent reaction between the condensate and substrate adatoms. It is assumed that this process is random in nature and that the higher index faces grow more rapidly than the lower index faces and will eventually disappear as is suggested in figure 10.
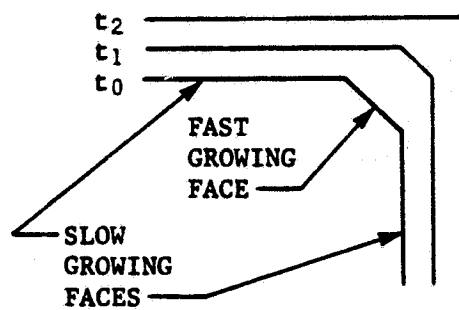
33

t_2
t_1
t_0

FAST
GROWING
FACE ——

SLOW
GROWING
FACES ——

Figure 10. Growth of crystal faces at times $t_0 < t_1 < t_2$.

PRELIMINARY COMPUTER RESULTS

A computer program following the flow chart in figure 6 was constructed. Time intervals of $\Delta t = 0.025$ and $\Delta t = 0.01$ were utilized for the deposition of adatoms, where deposition rates of 200 and 400 adatoms per second were used (1 μm/hr = 0.2778 nm/sec $\simeq$ 200 adatoms/sec for a 20 × 20 array). During each Δt time interval the surface adatoms were assigned a random energy from a Boltzmann distribution and the poten-tial energies were adjusted by using the potential masks of table 4. The potential changes in table 4 were approximated by assigning a value to ΔU_m and then calculating the nearest neighbor potential change ϕ_1 from the re-lation of equation (10). The other neighboring potential changes were calculated by assuming a (m_o, n_o) Mie potential where $\phi_2 = \alpha_2 \phi_1$ and $\phi_3 = \alpha_3 \phi_1$. These potential changes then produced $\phi_0 = \Sigma \phi_i$, which depends upon the particular orienta-tion being modeled.

Some preliminary results obtained from the computer simulations are given in the following figures. In these figures, the initial substrate geometry was assumed flat with a ledge of height one along the top row of a 20 × 20 array. Figure 11 illustrates the graphic display option of crystal growth that is available. Note in the center of this figure the critical cluster of size 4 for a (100) orientation of crystal growth. Figures 12(a) and (b) illustrate the vertical growth rate vs. time for various orienta-tions and migration levels. Note that for ΔU_m large (near ΔU_e) there is more evaporation of adatoms from the surface and consequently there is a lower growth rate. Note also that the (111) orientation has a larger growth rate than the (100) or (110) orientations.

ACKNOWLEDGMENTS
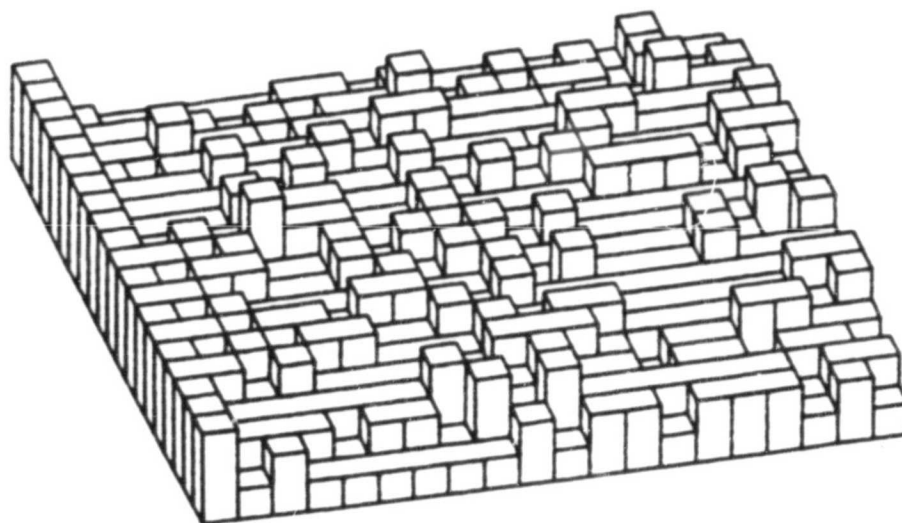
Figure 11.   Graphic display of crystal growth (100)
orientation.

Figure 12. Growth rate vs. time.

TIME, SECONDS

VERTICAL GROWTH RATE, NM/SECOND
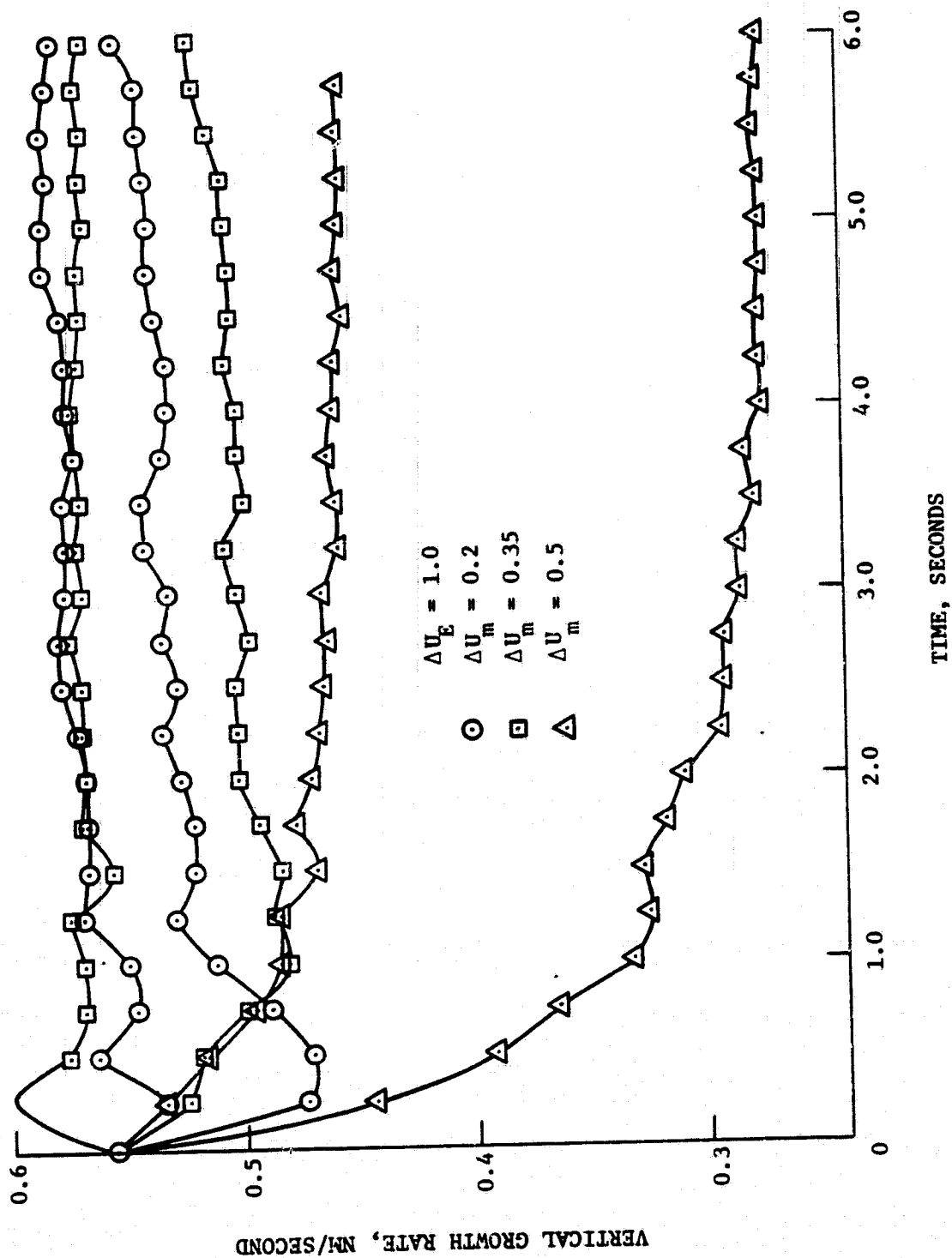
$\Delta U_E = 1.0$

$\Delta U_m = 0.2$

$\Delta U_m = 0.35$

$\Delta U_m = 0.5$

37

REFERENCES

1. Barton, W.K.; Gabrera, N.; and Frank, F.C.: The Growth of Crystals and the Equilibrium Structure of Their Surfaces. Phil. Trans. R. Soc. (London), Vol. 243A, 1951, pp. 299-358.

2. Gilmer, G.H.; and Bennema, P.: Simulation of Crystal Growth with Surface Diffusion. J. Appl. Phys., Vol. 43, No. 4, April 1972, pp. 1347-1360.

3. Abraham, F.F.; and White, G.M.: Computer Simulation of Vapor Deposition on Two-Dimensional Lattices. J. Appl. Phys., Vol. 41, No. 4, March 15, 1970, pp. 1841-1849.

4. Gilmer, G.H.: Simulation of Crystal Growth from the Vapor. Proc., 1976 Internat'l. Conf. on Computer Simulation for Materials Applications, April 19-26, 1976, Nat'l. Bureau of Standards (Gaithersburg, Md.), Arsenault, R.J.; Beller, J.R., Jr.,; and Simmons, J.A., eds.

5. Gilmer, G.H.: Computer Models of Crystal Growth. Science, Vol. 28, 1980, pp. 355-363.

6. Gilmer, G.H.: Transients in the Rate of Crystal Growth. J. Crystal Growth, Vol. 49, 1980, pp. 465-474.

7. Weeks, J.D.; and Gilmer, G.H.: Dynamics of Crystal Growth. In: Advances in Chemical Physics, Vol. 40, John Wiley & Sons (N.Y.), 1979.

8. Leamy, H.J.; Gilmer, G.H.; and Jackson, K.A.: Statistical Thermodynamics of Clean Surfaces. In: Surface Physics of Materials I. Blakely, J.M., ed., Academic Press (N.Y.), 1975.

9. Lewis, B.; Anderson, J.C.: Nucleation and Growth of Thin Films, Academic Press (N.Y.), 1978.

10. Chopra, K.L.: Thin Film Phenomena. McGraw Hill Book Company (N.Y.), 1969.

11. Walton, D.: Nucleation of Vapor Deposits. J. Chem. Phys., Vol. 37, No. 10, Nov. 1962, pp. 2182-2188.

12. Walton, D.; Rhodin, T.N.; and Rollins, R.W.: Nucleation of Silver on Sodium Chloride. J. Chem. Phys., Vol. 38, No. 11, June 1, 1963, pp. 2698-2704.

13. Flemings, M.C.: Solidification Processing. McGraw Hill Book Co. (N.Y.), 1974.